

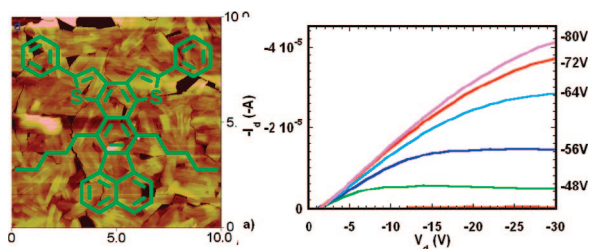
# Organic Semiconducting Materials from Sulfur-Hetero Benzo[*k*]fluoranthene Derivatives: Synthesis, Photophysical Properties, and Thin Film Transistor Fabrication

Qifan Yan,<sup>†</sup> Yan Zhou,<sup>†</sup> Ben-Bo Ni,<sup>†</sup> Yuguo Ma,<sup>\*,†</sup> Jian Wang,<sup>\*,‡</sup> Jian Pei,<sup>\*,†</sup> and Yong Cao<sup>‡</sup>

Beijing National Laboratory for Molecular Sciences (BNLMS), Key Laboratories of Bioorganic Chemistry and Molecular Engineering and of Polymer Chemistry and Physics of Ministry of Education, College of Chemistry, Peking University, Beijing 100871, and Institute of Polymer Optoelectronic Materials and Devices, South China University of Technology, and Key Laboratory of Specially Functional Materials of Ministry of Education, Guangzhou 510640, China

*jianpei@pku.edu.cn*

Received March 18, 2008



A new family of air-stable sulfur-hetero oligoarenes based on the benzo[*k*]fluoranthene unit has been facilely developed as the active materials for thin film organic field-effect transistors. The Diels–Alder reaction between cyclopentadienone **1** and 2,2'-(ethyne-1,2-diyl)bisthiophene followed by decarbonylation afforded fluoranthene derivative **2**. After bromination and subsequent substitution through Suzuki coupling reaction, the FeCl<sub>3</sub>-oxidative cyclization produced sulfur-hetero benzo[*k*]fluoranthene derivatives **8–12**. In dilute chloroform solution, the absorption and emission behaviors of **2** and **4–7** showed characteristic features of the fluoranthene units, while their emission  $\lambda_{\text{max}}$  red-shifted with an increase of the effective conjugation length. The steady state absorption and emission spectra of these newly synthesized compounds were thoroughly investigated and discussed. Thin film organic field-effect transistors (OFETs) using **8–11** as active materials were fabricated in a “top contact” configuration. Substituents at the skeleton play an important role in the film morphologies, which lead to different mobilities, while the charge mobilities of **8–11** from OFETs were improved after thermal annealing of the thin films. A carrier mobility as high as 0.083 cm<sup>2</sup> V<sup>-1</sup> s<sup>-1</sup> and current on/off ratio of 10<sup>6</sup> were achieved through vacuum-deposited film followed by the thermal annealing process from **11**.

## Introduction

Field-effect transistors (FETs) have been investigated intensively since their discovery in the 1960s owing to their important role in integrated circuits.<sup>1</sup> In comparison with inorganic semiconducting materials such as silicon, organic semiconductors can be easily processed with low cost and low temperature processing techniques, such as spin-casting and inkjet printing,<sup>2–4</sup> which enable large area electronics fabricated on a flexible

substrate. Moreover, their optoelectronic properties can be tuned through chemical engineering. Therefore, organic field-effect transistors (OFETs) have been extensively employed in organic-based electronic circuits to drive displays,<sup>5–8</sup> to operate sensors,<sup>9,10</sup> and so on.

Among various organic semiconductors for OFETs, pentacene is regarded as a promising candidate owing to its high hole mobility.<sup>11–13</sup> However, pentacene is rather unstable, especially under an electric field, and difficult to process due to its poor

<sup>†</sup> Peking University.

<sup>‡</sup> South China University of Technology.

(1) Murphy, A. R.; Fréchet, J. M. J. *Chem. Rev.* **2007**, *107*, 1066–1096.

(2) Chen, J.; Leblanc, V.; Kang, S. H.; Benning, P. J.; Schut, D.; Baldo, M. A.; Schmidt, M. A.; Bulović, V. *Adv. Func. Mater.* **2007**, *17*, 2722–2727.

(3) Forrest, S. R. *Nature* **2004**, *428*, 911–918.

solubility in common organic solvents, which limited its applications in organic optoelectronics. In the past decade, considerable research efforts have been devoted to develop pentacene derivatives with higher solubility and stability.<sup>11,14–20</sup> Although significant achievements have been made in both the development of new organic materials and the optimization of techniques for device fabrication,<sup>2,21–40</sup> it is still a challenging task to understand the structure–property relationship through developing stable organic  $\pi$ -conjugated small molecules for thin film-based OFETs with good charge carrier mobilities. Recent progress has demonstrated thiophene-based molecules as a novel

class of promising organic semiconductors for OFETs.<sup>16,41–72</sup> Since thiophene derivatives can be easily chemically modified and exhibit good thermal stabilities, various thiophene-containing structures have been synthesized.<sup>28,41–45,48,49,57,69–71,73–86</sup>

- (4) Dimitrakopoulos, C. D.; Malenfant, P. R. L. *Adv. Mater.* **2002**, *14*, 99–117.
- (5) Wisniewski, R. *Nature* **1998**, *394*, 225–227.
- (6) Comiskey, B.; Albert, J. D.; Yoshizawa, H.; Jacobson, J. *Nature* **1998**, *394*, 253–255.
- (7) Mitschke, U.; Bäuerle, P. *J. Mater. Chem.* **2000**, *10*, 1471–1507.
- (8) Andersson, P.; Forchheimer, R.; Tehrani, P.; Berggren, M. *Adv. Func. Mater.* **2007**, *17*, 3074–3082.
- (9) Lin, Y. R.; Dodabalapur, A.; Sarpeshkar, R.; Bao, Z.; Li, W.; Baldwin, K.; Raju, V. R.; Katz, H. E. *Appl. Phys. Lett.* **1999**, *74*, 2714–2716.
- (10) Crone, B.; Dodabalapur, A.; Lin, Y.-Y.; Filas, R. W.; Bao, Z.; LaDuca, A.; Sarpeshkar, R.; Katz, H. E.; Li, W. *Nature* **2000**, *403*, 521–523.
- (11) Meng, H.; Bendikov, M.; Mitchell, G.; Helgeson, R.; Wudl, F.; Bao, Z.; Siegrist, T.; Kloc, C.; Chen, C.-H. *Adv. Mater.* **2003**, *15*, 1090–1093.
- (12) Nelson, S. F.; Lin, Y.-Y.; Gundlach, D. J.; Jackson, T. N. *Appl. Phys. Lett.* **1998**, *72*, 1854–1856.
- (13) Lin, Y.-Y.; Gundlach, D. J.; Nelson, S. F.; Jackson, T. N. *IEEE Electron Device Lett.* **1997**, *18*, 606–608.
- (14) Afzali, A.; Dimitrakopoulos, C. D.; Breen, T. L. *J. Am. Chem. Soc.* **2002**, *124*, 8812–8813.
- (15) Payne, M. M.; Parkin, S. R.; Anthony, J. E.; Kuo, C.-C.; Jackson, T. N. *J. Am. Chem. Soc.* **2005**, *127*, 4986–4987.
- (16) Brisenno, A. L.; Miao, Q.; Ling, M.-M.; Reese, C.; Meng, H.; Bao, Z.; Wudl, F. *J. Am. Chem. Soc.* **2006**, *128*, 15576–15577.
- (17) Tang, M. L.; Okamoto, T.; Bao, Z. *J. Am. Chem. Soc.* **2006**, *128*, 16002–16003.
- (18) Okamoto, T.; Bao, Z. *J. Am. Chem. Soc.* **2007**, *129*, 10308–10309.
- (19) Brisenno, A. L.; Mannsfeld, S. C. B.; Lu, X.; Xiong, Y.; Jenekhe, S. A.; Bao, Z.; Xia, Y. *Nano Lett.* **2007**, *7*, 668–675.
- (20) Swartz, C. R.; Parkin, S. R.; Bullock, J. E.; Anthony, J. E.; Mayer, A. C.; Malliaras, G. G. *Org. Lett.* **2005**, *7*, 3163–3166.
- (21) Xu, B.; Xiao, X.; Yang, X.; Zang, L.; Tao, N. *J. Am. Chem. Soc.* **2005**, *127*, 2386–2387.
- (22) Che, Y.; Datar, A.; Yang, X.; Naddo, T.; Zhao, J.; Zang, L. *J. Am. Chem. Soc.* **2007**, *129*, 6354–6355.
- (23) Pisula, W.; Menon, A.; Stepputat, M.; Lieberwirth, I.; Kolb, U.; Tracz, A.; Siringhaus, H.; Pakula, T.; Müllen, K. *Adv. Mater.* **2005**, *17*, 684–689.
- (24) Brisenno, A. L.; Tseng, R. J.; Ling, M.-M.; Falcao, E. H. L.; Yang, Y.; Wudl, F.; Bao, Z. *Adv. Mater.* **2006**, *18*, 2320–2324.
- (25) Coropceanu, V.; Cornil, J.; da Silva Fiho, D. A.; Olivier, Y.; Silbey, R.; Brédas, J.-L. *Chem. Rev.* **2007**, *107*, 926–952.
- (26) Goldmann, C.; Haas, S.; Krellner, C.; Pernstich, K. P.; Gundlach, D. J.; Batlogg, B. *J. Appl. Phys.* **2004**, *96*, 2080–2086.
- (27) Brisenno, A. L.; Mannsfeld, S. C. B.; Ling, M. M.; Liu, S.; Tseng, R. J.; Reese, C.; Roberts, M. E.; Yang, Y.; Wudl, F.; Bao, Z. *Nature* **2006**, *444*, 913–917.
- (28) Zhou, Y.; Liu, W.-J.; Ma, Y.; Wang, H.; Qi, L.; Cao, Y.; Wang, J.; Pei, J. *J. Am. Chem. Soc.* **2007**, *129*, 12386–12387.
- (29) Shtein, M.; Peumans, P.; Benziger, J. B.; Forrest, S. R. *Adv. Mater.* **2004**, *16*, 1615–1620.
- (30) Maunoury, J. C.; Howse, J. R.; Turner, M. L. *Adv. Mater.* **2007**, *19*, 805–809.
- (31) Wang, Z.; Zhang, J.; Xing, R.; Yuan, J.; Yan, D.; Han, Y. *J. Am. Chem. Soc.* **2003**, *125*, 15278–15279.
- (32) Wu, Y.; Li, Y.; Ong, B. S. *J. Am. Chem. Soc.* **2007**, *129*, 1862–1863.
- (33) Wu, Y.; Li, Y.; Ong, B. S. *J. Am. Chem. Soc.* **2006**, *128*, 4202–4203.
- (34) Wu, Y.; Li, Y.; Liu, P.; Gardner, S.; Ong, B. S. *Chem. Mater.* **2006**, *18*, 4627–4632.
- (35) Li, Y.; Wu, Y.; Ong, B. S. *J. Am. Chem. Soc.* **2005**, *127*, 3266–3267.
- (36) Liu, P.; Wu, Y.; Li, Y.; Ong, B. S.; Zhu, S. *J. Am. Chem. Soc.* **2006**, *128*, 4554–4555.
- (37) Brisenno, A. L.; Roberts, M.; Ling, M.-M.; Moon, H.; Nemanick, E. J.; Bao, Z. *J. Am. Chem. Soc.* **2006**, *128*, 3880–3881.
- (38) Park, S. Y.; Kwon, T.; Lee, H. H. *Adv. Mater.* **2006**, *18*, 1861–1864.
- (39) Yu, H.; Luo, Y.; Beverly, K.; Stoddart, J. F.; Tseng, H.-R.; Heath, J. R. *Angew. Chem., Int. Ed.* **2003**, *42*, 5706–5711.
- (40) Di, C.-a.; Yu, G.; Liu, Y.; Xu, X.; Wei, D.; Song, Y.; Sun, Y.; Wang, Y.; Zhu, D.; Liu, J.; Liu, X.; Wu, D. X. *J. Am. Chem. Soc.* **2006**, *128*, 16418–16419.
- (41) Katz, H. E.; Laquindanum, J. G.; Lovinger, A. J. *Chem. Mater.* **1998**, *10*, 633–638.
- (42) Halik, M.; Klauk, H.; Zschieschang, U.; Schmid, G.; Ponomarenko, S.; Kirchmeyer, S.; Weber, W. *Adv. Mater.* **2003**, *15*, 917–922.
- (43) Mushrush, M.; Facchetti, A.; Lefenfeld, M.; Katz, H. E.; Marks, T. J. *J. Am. Chem. Soc.* **2003**, *125*, 9414–9423.
- (44) Takimiya, K.; Kunugi, Y.; Toyoshima, Y.; Otsubo, T. *J. Am. Chem. Soc.* **2005**, *127*, 3605–3612.
- (45) Takimiya, K.; Ebata, H.; Sakamoto, K.; Izawa, T.; Otsubo, T.; Kunugi, Y. *J. Am. Chem. Soc.* **2006**, *128*, 12604–12605.
- (46) Xiao, K.; Liu, Y.; Qi, T.; Zhang, W.; Wang, F.; Gao, J.; Qiu, W.; Ma, Y.; Cui, G.; Chen, S.; Zhan, X.; Yu, G.; Qin, J.; Hu, W.; Zhu, D. *J. Am. Chem. Soc.* **2005**, *127*, 13281–13286.
- (47) Sun, Y.; Tan, L.; Jiang, S.; Qian, H.; Wang, Z.; Yan, D.; Di, C.; Wang, Y.; Wu, W.; Yu, G.; Yan, S.; Wang, C.; Hu, W.; Liu, Y.; Zhu, D. *J. Am. Chem. Soc.* **2007**, *129*, 1882–1883.
- (48) Valiyev, F.; Hu, W.-S.; Chen, H.-Y.; Kuo, M.-Y.; Chao, I.; Tao, Y.-T. *Chem. Mater.* **2007**, *19*, 3018–3026.
- (49) Yoon, M.-H.; DiBenedetto, S. A.; Facchetti, A.; Marks, T. J. *J. Am. Chem. Soc.* **2005**, *127*, 1348–1349.
- (50) Yoon, M.-H.; DiBenedetto, S. A.; Russell, M. T.; Facchetti, A.; Marks, T. J. *Chem. Mater.* **2007**, *19*, 4864–4881.
- (51) Naraso; Nishida, J.-i.; Ando, S.; Yamaguchi, J.; Itaka, K.; Koinuma, H.; Tada, H.; Tokito, S.; Yamashita, Y. *J. Am. Chem. Soc.* **2005**, *127*, 10142–10143.
- (52) Naraso; Nishida, J.-i.; Kumaki, D.; Tokito, S.; Yamashita, Y. *J. Am. Chem. Soc.* **2006**, *128*, 9598–9599.
- (53) Lee, J.; Panzer, M. J.; He, Y.; Lodge, T. P.; Frisbie, C. D. *J. Am. Chem. Soc.* **2007**, *129*, 4532–4533.
- (54) Tian, H.; Shi, J.; He, B.; Hu, N.; Dong, S.; Yan, D.; Zhang, J.; Geng, Y.; Wang, F. *Adv. Func. Mater.* **2007**, *17*, 1940–1951.
- (55) Wu, Y.; Liu, P.; Gardner, S.; Ong, B. S. *Chem. Mater.* **2005**, *17*, 221–223.
- (56) Vidolot-Ackermann, C.; Ackermann, J.; Brisset, H.; Kawamura, K.; Yoshimoto, N.; Raynal, P.; El Kassim, A.; Fages, F. *J. Am. Chem. Soc.* **2005**, *127*, 16346–16347.
- (57) Letizia, J. A.; Facchetti, A.; Stern, C. L.; Ratner, M. A.; Marks, T. J. *J. Am. Chem. Soc.* **2005**, *127*, 13476–13477.
- (58) Zhang, M.; Tsao, H. N.; Pisula, W.; Yang, C.; Mishra, A. K.; Müllen, K. *J. Am. Chem. Soc.* **2007**, *129*, 3472–3473.
- (59) Pan, H.; Li, Y.; Wu, Y.; Liu, P.; Ong, B. S.; Zhu, S.; Xu, G. *Chem. Mater.* **2006**, *18*, 3237–3241.
- (60) Pan, H.; Wu, Y.; Li, Y.; Liu, P.; Ong, B. S.; Zhu, S.; Xu, G. *Adv. Func. Mater.* **2007**, *17*, 3574–3579.
- (61) Kim, K. H.; Chi, Z.; Cho, M. J.; Jin, J.-I.; Cho, M. Y.; Kim, S. J.; Joo, J.-s.; Choi, D. H. *Chem. Mater.* **2007**, *19*, 4925–4932.
- (62) Ong, B. S.; Wu, Y.; Liu, P.; Gardner, S. *J. Am. Chem. Soc.* **2004**, *126*, 3378–3379.
- (63) Zen, A.; Saphiannikova, M.; Neher, D.; Asawapirom, U.; Scherf, U. *Chem. Mater.* **2005**, *17*, 781–786.
- (64) Meng, H.; Zheng, J.; Lovinger, A. J.; Wang, B.-C.; Van Patten, P. G.; Bao, Z. *Chem. Mater.* **2003**, *15*, 1778–1787.
- (65) Katz, H. E.; Dodabalapur, A.; Torsi, L.; Elder, D. *Chem. Mater.* **1995**, *7*, 2238–2240.
- (66) Merlo, J. A.; Newman, C. R.; Gerlach, C. P.; Kelley, T. W.; Muires, D. V.; Fritz, S. E.; Toney, M. F.; Frisbie, C. D. *J. Am. Chem. Soc.* **2005**, *127*, 3997–4009.
- (67) Mas-Torrent, M.; Durkut, M.; Hadley, P.; Ribas, X.; Rovira, C. *J. Am. Chem. Soc.* **2004**, *126*, 984–985.
- (68) Kono, T.; Kumaki, D.; Nishida, J.-i.; Sakanoue, T.; Kakita, M.; Tada, H.; Tokito, S.; Yamashita, Y. *Chem. Mater.* **2007**, *19*, 1218–1220.
- (69) Usta, H.; Lu, G.; Facchetti, A.; Marks, T. J. *J. Am. Chem. Soc.* **2006**, *128*, 9034–9035.
- (70) Zen, A.; Pingel, P.; Jaiser, F.; Neher, D.; Grenzer, J.; Zhuang, W.; Rabe, J. P.; Bilge, A.; Galbrecht, F.; Nehls, B. S.; Farrell, T.; Scherf, U.; Abellon, R. D.; Grozema, F. C.; Siebbeles, L. D. A. *Chem. Mater.* **2007**, *19*, 1267–1276.
- (71) Laquindanum, J. G.; Katz, H. E.; Lovinger, A. J. *J. Am. Chem. Soc.* **1998**, *120*, 664–672.
- (72) Zen, A.; Bilge, A.; Galbrecht, F.; Alle, R.; Meerholz, K.; Grenzer, J.; Neher, D.; Scherf, U.; Farrell, T. *J. Am. Chem. Soc.* **2006**, *128*, 3914–3915.
- (73) Facchetti, A.; Deng, Y.; Wang, A.; Koide, Y.; Siringhaus, H.; Marks, T. J.; Friend, R. H. *Angew. Chem., Int. Ed.* **2000**, *39*, 4547–4551.
- (74) Li, Y.; Wu, Y.; Liu, P.; Birau, M.; Pan, H.; Ong, B. S. *Adv. Mater.* **2006**, *18*, 3029–3032.
- (75) Li, X.-C.; Siringhaus, H.; Garnier, F.; Holmes, A. B.; Moratti, S. C.; Feeder, N.; Clegg, W.; Teat, S. J.; Friend, R. H. *J. Am. Chem. Soc.* **1998**, *120*, 2206–2207.
- (76) Takimiya, K.; Kunugi, Y.; Konda, Y.; Niihara, N.; Otsubo, T. *J. Am. Chem. Soc.* **2004**, *126*, 5084–5085.

Moreover, discotic polycyclic aromatic hydrocarbons (PAHs) such as hexabenzocoronenes (HBCs) and perylene derivatives were also employed as active materials for OFETs.<sup>20,23,87–93</sup>

Since both the molecular size and shape of oligoarenes play very important roles in their electronic properties and assembly, it is necessary to design and synthesize oligoarenes with diverse structures for systematic investigation of their structure–property relationships and specific applications.<sup>1,47,54,87,93–106</sup> In our previous contributions, we reported several  $\pi$ -extended, condensed, sulfur-rich benzothiophenes favoring  $\pi$ - $\pi$  interaction. Such oligoarenes can easily form bulk quantity individual microwires through self-assembly. The organic transistors based on these molecules with the mobility of  $0.01 \text{ cm}^2 \text{ V}^{-1} \text{ s}^{-1}$  were successfully achieved, demonstrating that such a processing strategy for air-stable  $\pi$ -extended condensed benzothiophenes with good performance is quite attractive.<sup>28,107</sup> Theoretical calculations and experimental results suggest that the charge

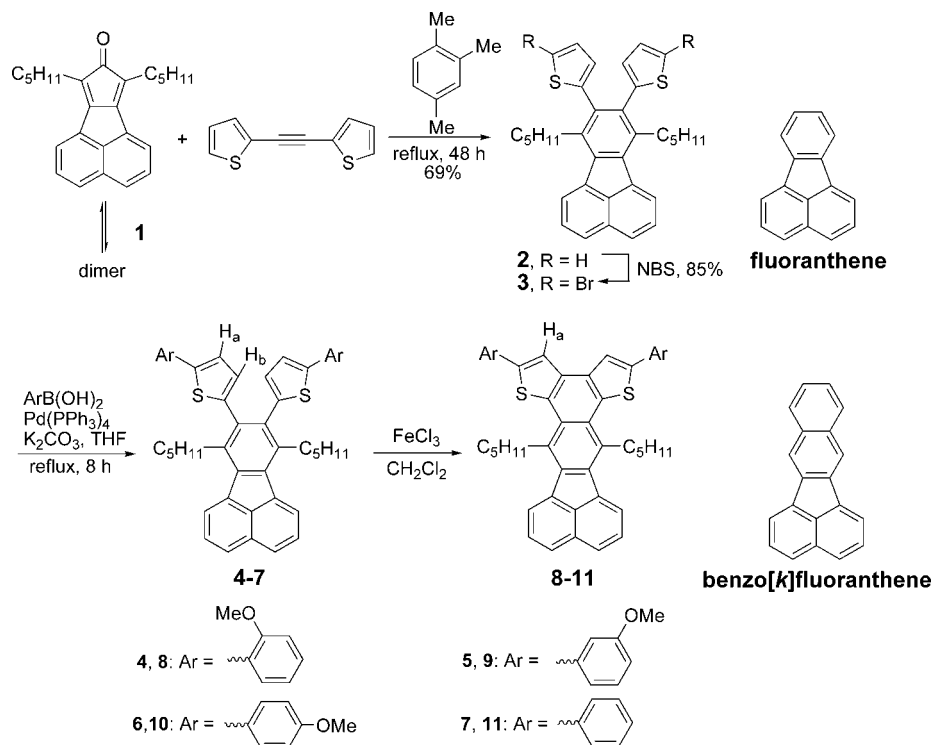
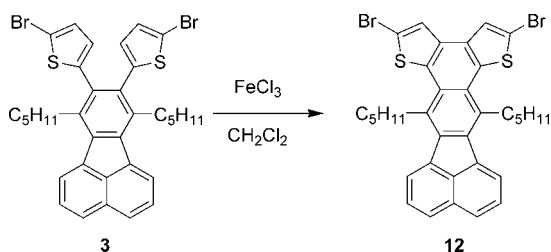
carrier transporting is usually maximized along the  $\pi$ -stacking orientation.<sup>22,25,108</sup> Fluoranthene and benzo[*k*]fluoranthene derivatives have previously been employed to serve as the basic skeleton to prepare a blue-light emitter for organic light-emitting diodes (OLEDs).<sup>109</sup> Such a  $\pi$ -extended planar core containing sulfur atoms is employed to facilitate molecular self-association driven by  $\pi$ - $\pi$  stacking. Herein, we report the synthesis of a family of novel hetero oligoarenes based on fluoranthene and benzo[*k*]fluoranthene unit with good stability in air. We have developed an expedient route to target molecules **8–11** in four-step reaction sequences. Fused thiophene aromatic compounds were developed as new organic semiconductors to avoid sterically induced twist between proximal aromatic rings. Such large planar conjugated molecules with flexible side chains provide a variety of intra- and intermolecular interactions in these thiophene-based materials, such as van der Waals interactions,  $\pi$ - $\pi$  stacking, and sulfur–sulfur interactions, to essentially achieve high charge carrier mobilities.<sup>47,102,110,111</sup> The compounds reported herein combine the elements of oligoarenes and peripheral sulfur atoms, which, we speculate, would be beneficial to device performance in OFETs. All compounds exhibit good thermal and oxidative stability in air. The thermal annealing process was conducted directly after vacuum-depositing the material onto the cold, *n*-octadecyltrichlorosilane (OTS) treated substrate. Crystalline films were obtained, and an increase in the mobility of several orders of magnitude and on/off ratio was achieved with such a technique. It is a promising, efficient technique to fabricate OFETs. Thermal annealing was employed to improve transistor performances, which is seldomly used for crystalline small molecular materials. The thin film transistors with carrier mobility of  $0.083 \text{ cm}^2 \text{ V}^{-1} \text{ s}^{-1}$  are realized from **11**.

## Results and Discussion

**Synthesis and NMR Characterization.** Scheme 1 illustrates the synthetic approach to the designed sulfur-hetero benzo[*k*]fluoranthene derivatives **8–11**. Cyclopentadienone **1**, which is usually in equilibrium with its dimer, was obtained as a light yellow solid in good yield according to the literature.<sup>112</sup> The Diels–Alder reaction between cyclopentadienone **1** and 2,2'-(ethyne-1,2-diyl)bisthiophene followed by decarbonylation in refluxed 1,2,4-trimethylbenzene produced **2** in 69% yield. Prior to the oxidative cyclization by  $\text{FeCl}_3$  to form the carbon–carbon bond at  $\beta$ -positions of the thiophene rings, the  $\alpha$ -positions of thiophene units were brominated. The reasons for this bromination are as follows. First, it protected  $\alpha$ -positions of thiophene rings from polymerization caused by its high reactivity. Second, the bromide functionality provided the convenience to obtain the corresponding derivatives through various cross-coupling reactions. As shown in Scheme 1, the bromination of **2** by NBS afforded **3** in 85% yield.<sup>113</sup> The Suzuki coupling between **3** and

- (77) Heeney, M.; Bailey, C.; Genevicius, K.; Shkunov, M.; Sparrowe, D.; Tierney, S.; McCulloch, I. *J. Am. Chem. Soc.* **2005**, *127*, 1078–1079.  
 (78) Meng, H.; Sun, F.; Goldfinger, M. B.; Jaycox, G. D.; Li, Z.; Marshall, W. J.; Blackman, G. S. *J. Am. Chem. Soc.* **2005**, *127*, 2406–2407.  
 (79) Ando, S.; Murakami, R.; Nishida, J.-i.; Tada, H.; Inoue, Y.; Tokito, S.; Yamashita, Y. *J. Am. Chem. Soc.* **2005**, *127*, 14996–14997.  
 (80) Mas-Torrent, M.; Hadley, P.; Bromley, S. T.; Ribas, X.; Tarrés, J.; Mas, M.; Molins, E.; Veciana, J.; Rovira, C. *J. Am. Chem. Soc.* **2004**, *126*, 8546–8553.  
 (81) Pan, H.; Li, Y.; Wu, Y.; Liu, P.; Ong, B. S.; Zhu, S.; Xu, G. *J. Am. Chem. Soc.* **2007**, *129*, 4112–4113.  
 (82) Dhoot, A. S.; Yuen, J. D.; Heeney, M.; McCulloch, I.; Moses, D.; Heeger, A. J. *Proc. Natl. Acad. Sci. U.S.A.* **2006**, *103*, 11834–11837.  
 (83) Yamamoto, T.; Takimiya, K. *J. Am. Chem. Soc.* **2007**, *129*, 2224–2225.  
 (84) Chesterfield, R. J.; Newman, C. R.; Pappenfus, T. M.; Ewbank, P. C.; Haukaas, M. H.; Mann, K. R.; Miller, L. L.; Frisbie, C. D. *Adv. Mater.* **2003**, *15*, 1278–1282.  
 (85) Handa, S.; Miyazaki, E.; Takimiya, K.; Kunugi, Y. *J. Am. Chem. Soc.* **2007**, *129*, 11684–11685.  
 (86) Videtot, C.; Ackermann, J.; Blanchard, P.; Raimundo, J.-M.; Frère, P.; Allain, M.; de Bettignies, R.; Levillain, E.; Roncali, J. *Adv. Mater.* **2003**, *15*, 306–310.  
 (87) Xiao, S.; Myers, M.; Miao, Q.; Sanaur, S.; Pang, K.; Steigerwald, M. L.; Nuckolls, C. *Angew. Chem., Int. Ed.* **2005**, *44*, 7390–7394.  
 (88) Wang, H.; Zhu, F.; Yang, J.; Geng, Y.; Yan, D. *Adv. Mater.* **2007**, *19*, 2168–2171.  
 (89) Babel, A.; Jenekhe, S. A. *J. Am. Chem. Soc.* **2003**, *125*, 13656–13657.  
 (90) Shklyarevskiy, I. O.; Jonkheijm, P.; Stutzmann, N.; Wasserberg, D.; Wondergem, H. J.; Christiaan, P. C. M.; Schenning, A. P. H. J.; de Leeuw, D. M.; Tomović, Z.; Wu, J. S.; Müllen, K.; Maan, J. C. *J. Am. Chem. Soc.* **2005**, *127*, 16233–16237.  
 (91) Briseno, A. L.; Mannsfeld, S. C. B.; Reese, C.; Hancock, J. M.; Xiong, Y.; Jenekhe, S. A.; Bao, Z.; Xia, Y. *Nano Lett.* **2007**, *7*, 2847–2853.  
 (92) Xiao, S.; Tang, J.; Beetz, T.; Guo, X.; Tremblay, N.; Siegrist, T.; Zhu, Y.; Steigerwald, M.; Nuckolls, C. *J. Am. Chem. Soc.* **2006**, *128*, 10700–10701.  
 (93) Schmidt-Mende, L.; Fechtenkötter, A.; Müllen, K.; Moons, E.; Friend, R. H.; MacKenzie, J. D. *Science* **2001**, *293*, 1119–1122.  
 (94) Kunugi, Y.; Takimiya, K.; Negishi, N.; Otsubo, T.; Aso, Y. *J. Mater. Chem.* **2004**, *14*, 2840–2841.  
 (95) Amriou, S.; Mehta, A.; Bryce, M. R. *J. Mater. Chem.* **2005**, *15*, 1232–1234.  
 (96) Ito, K.; Suzuki, T.; Sakamoto, Y.; Kubota, D.; Inoue, Y.; Sato, F.; Tokito, S. *Angew. Chem., Int. Ed.* **2003**, *42*, 1159–1162.  
 (97) Song, Y.; Di, C.; Yang, X.; Li, S.; Xu, W.; Liu, Y.; Yang, L.; Shuai, Z.; Zhang, D.; Zhu, D. *J. Am. Chem. Soc.* **2006**, *128*, 15940–15941.  
 (98) Sundar, V. C.; Zaumseil, J.; Podzorov, V.; Menard, E.; Willett, R. L.; Someya, T.; Gershenson, M. E.; Rogers, J. A. *Science* **2004**, *303*, 1644–1646.  
 (99) Hagen, S.; Hopf, H. *Top. Curr. Chem.* **1998**, *196*, 45–89.  
 (100) Randić, M. *Chem. Rev.* **2003**, *103*, 3449–3605.  
 (101) Bruns, D.; Miura, H.; Vollhardt, K. P. C.; Stanger, A. *Org. Lett.* **2003**, *5*, 549–552.  
 (102) Motoyanagi, J.; Fukushima, T.; Ishii, N.; Aida, T. *J. Am. Chem. Soc.* **2006**, *128*, 4220–4221.  
 (103) Yamamoto, Y.; Fukushima, T.; Suna, Y.; Ishii, N.; Saeki, A.; Seki, S.; Tagawa, S.; Taniguchi, M.; Kawai, T.; Aida, T. *Science* **2006**, *314*, 1761–1764.  
 (104) Katz, H. E.; Bao, Z.; Gilat, S. L. *Acc. Chem. Res.* **2001**, *34*, 359–369.  
 (105) Chen, H. Z.; Ling, M. M.; Mo, X.; Shi, M. M.; Wang, M.; Bao, Z. *Chem. Mater.* **2007**, *19*, 816–824.  
 (106) Jones, B. A.; Facchetti, A.; Wasielewski, M. R.; Marks, T. J. *J. Am. Chem. Soc.* **2007**, *129*, 15259–15278.

- (107) Liu, W.-J.; Zhou, Y.; Ma, Y.; Cao, Y.; Wang, J.; Pei, J. *Org. Lett.* **2007**, *9*, 4187–4190.  
 (108) Lemaire, V.; Da Silva Filho, D. A.; Coropceanu, V.; Lehmann, M.; Geerts, Y.; Piris, J.; Debije, M. G.; van de Craats, A. M.; Senthilkumar, K.; Siebbeles, L. D. A.; Warman, J. M.; Brédas, J.-L.; Cornil, J. *J. Am. Chem. Soc.* **2004**, *126*, 3271–3279.  
 (109) Chiechi, R. C.; Tseng, R. J.; Marchioni, F.; Yang, Y.; Wudl, F. *Adv. Mater.* **2006**, *18*, 325–328.  
 (110) de Bettignies, R.; Nicolas, Y.; Blanchard, P.; Levillain, E.; Nunzi, J.-M.; Roncali, J. *Adv. Mater.* **2003**, *15*, 1939–1943.  
 (111) Nicolas, Y.; Blanchard, P.; Levillain, E.; Allain, M.; Mercier, N.; Roncali, J. *Org. Lett.* **2004**, *6*, 273–276.  
 (112) Allen, C. F. H.; VanAllan, J. A. *J. Org. Chem.* **1952**, *17*, 845–854.

SCHEME 1. Synthesis of Benzo[*k*]fluoranthene Derivatives 8–11 and Structure of Fluoranthene and Benzo[*k*]fluorantheneSCHEME 2. Synthesis of Benzo[*k*]fluoranthene Model 12

phenylboronic acid or methoxyphenylboronic acids produced **4–7** in 85–92% yield, respectively. Optimizing the oxidative cyclization by examining the amount of FeCl<sub>3</sub> added as well as the reaction temperature, the oxidative cyclization protocol described in our previous contributions<sup>28,106,113,114</sup> was followed to construct the benzo[*k*]fluoranthene skeleton via thienyl–thienyl carbon–carbon bond formation and afforded **8–11** in 79–96% yield. Compound **12** as a model was also prepared through the same oxidative cyclization reaction from **3** as shown in Scheme 2. <sup>1</sup>H NMR was employed to monitor oxidative cyclization reactions. Two main transformations were found to be strong evidences to support carbon–carbon bond formation: first, two resonance signals of the protons in thiophene rings converted into one single peak downfield; second, the resonance signals of the α-CH<sub>2</sub> of the alkyl chains became broader and shifted downfield after oxidative cyclization reactions. The signals of H<sub>b</sub> exhibited almost the same chemical shift at about 6.75 ppm for **4–7** and disappeared in the <sup>1</sup>H NMR spectra of **8–11**. In the <sup>1</sup>H NMR spectrum of **4**, the signal assigned to H<sub>a</sub> was at chemical shift of 7.33 ppm as a duplet. After the cyclization, such a signal converted to a singlet and moved ca. 0.94 ppm

downfield as shown in the <sup>1</sup>H NMR spectrum of **8**. A similar downfield shift (ca. 0.9 ppm) of H<sub>a</sub> was also observed in <sup>1</sup>H NMR spectra of the other three compounds. The data clearly indicate the formation of the large polycyclic aromatic planar π-system after the cyclization (see the Supporting Information). All compounds were readily soluble in common organic solvents, such as CH<sub>2</sub>Cl<sub>2</sub>, CHCl<sub>3</sub>, and THF.

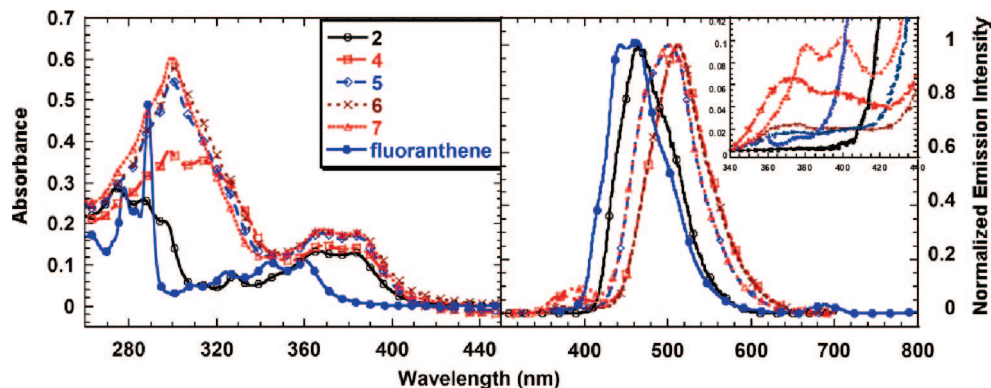
**Photophysical Properties in Solutions.** Figure 1 shows the absorption spectra of **2** and **4–7** in dilute chloroform (CHCl<sub>3</sub>) solutions (1.0 × 10<sup>-5</sup> M) in comparison with that of fluoranthene. The absorption spectrum of fluoranthene in dilute solution exhibited two major bands with absorption λ<sub>max</sub> at about 289 and 360 nm.<sup>115</sup> In comparison with fluoranthene, the absorption spectrum of **2** in dilute CHCl<sub>3</sub> solution also showed two major bands with absorption λ<sub>max</sub> at about 287 and 383 nm. As shown in Figure 1, **4–7** exhibited two major bands with absorption λ<sub>max</sub> at about 300 and 380 nm, which showed almost the same behaviors at the absorption band at 380 nm as that of **2**. Although the absorption bands of **4–7** at 380 nm were not affected by the introduction of the phenyl ring, their absorption bands at about 300 nm became very broad in comparison with that of **2**.

Figure 1 also shows the emission spectra of **2** and **4–7** in dilute chloroform solutions (1.0 × 10<sup>-5</sup> M). The emission spectrum of **2** peaked at 467 nm, which slightly red-shifted caused by thiophene ring substituents compared to those of fluoranthene (443 and 463 nm).<sup>115</sup> Compound **4** showed almost the same emission behaviors as **6**, and the emission spectra of **5** and **7** were approximately identical. In comparison with that of **2**, the emission λ<sub>max</sub> red-shifted about 33 nm to ca. 500 nm for **5** and **7** and about 43 nm to ca. 510 nm for **4** and **6**, respectively. The emission λ<sub>max</sub> of **4** and **6** red-shifted about 10 nm compared to those of **5** and **7**.

Figure 2 shows the absorption spectra of **8–12** in dilute chloroform solutions (1.0 × 10<sup>-5</sup> M), in which the benzo[*k*-

(113) Pei, J.; Zhang, W.-Y.; Mao, J.; Zhou, X.-H. *Tetrahedron Lett.* **2006**, *47*, 1551–1554.

(114) Zhou, Y.; Liu, W.-J.; Zhang, W.; Cao, X.-Y.; Zhou, Q.-F.; Ma, Y.; Pei, J. *J. Org. Chem.* **2006**, *71*, 6822–6828.



**FIGURE 1.** Absorption and emission spectra of 2, 4–7, and fluorene in dilute  $\text{CHCl}_3$  solutions ( $1.0 \times 10^{-5}$  M). The emission spectra were recorded using the following excitation wavelengths: 274 nm for 2; 298 nm for 4; 300 nm for 5; 290 nm for 6; and 296 nm for 7.

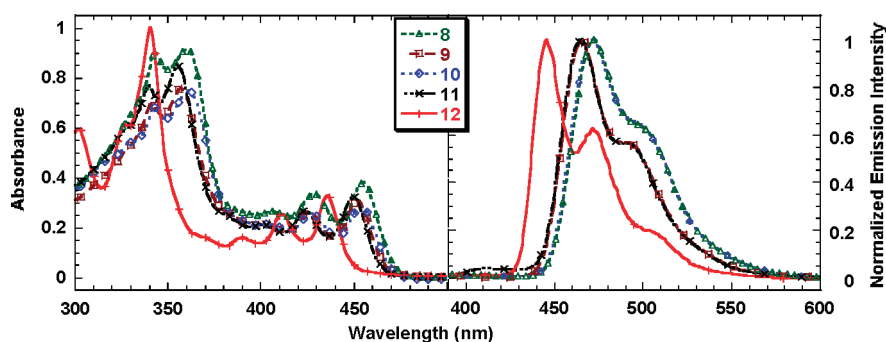


**FIGURE 2.** Absorption and emission spectra of compounds 8–12 in dilute  $\text{CHCl}_3$  solutions ( $1.0 \times 10^{-5}$  M). The emission spectra were recorded using the following excitation wavelengths: 474 nm for 8; 492 nm for 9; 479 nm for 10; and 474 nm for 11.

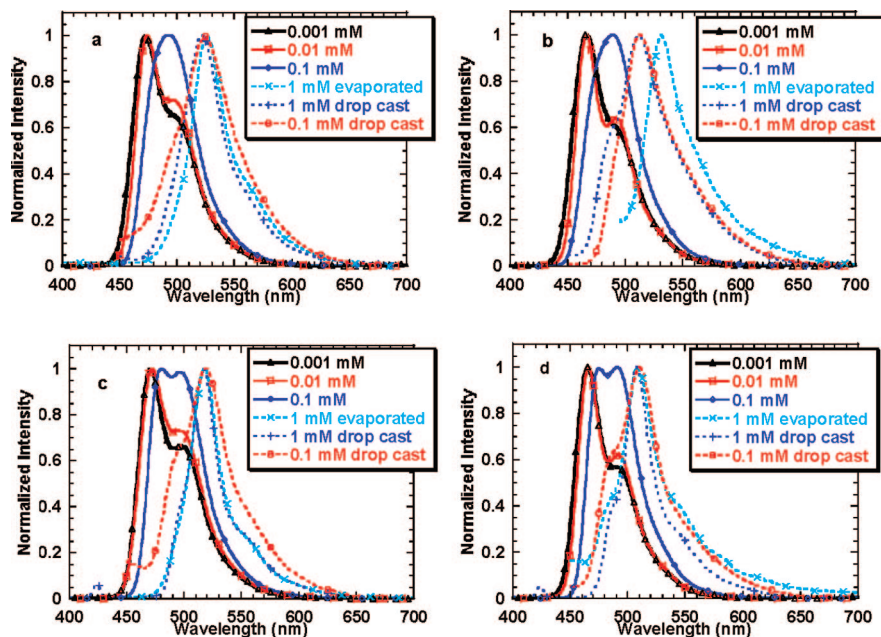


**FIGURE 3.** Fluorescence spectra of 8 (a), 9 (b), 10 (c), and 11 (d) in chloroform solutions with different concentrations and in the solid state.

]fluorene unit was constructed by the C–C bond formation between two thiophene units. Semiconductors 8–11 demonstrated very similar absorption and emission behavior, due to the same skeleton in their molecular structures. For 12, its absorption spectra exhibited two major bands with absorption  $\lambda_{\text{max}}$  at about 341 and 436 nm, which dramatically red-shifted in comparison with those of fluorene. Such a red-shift was attributed to the larger polycyclic aromatic benzo[*k*]fluorene  $\pi$ -planar system. Three vibronic bands were observed with

absorption  $\lambda_{\text{max}}$  at 390 ( $25\,641\text{ cm}^{-1}$ ), 411 ( $24\,330\text{ cm}^{-1}$ ), and 436 nm ( $22\,936\text{ cm}^{-1}$ ) for 12. The vibrational energy levels in the excited state of 12 appeared to be equally spaced with a wavenumber separation of about  $1394\text{ cm}^{-1}$ , which is expected from the theoretical model of an anharmonic oscillator.<sup>116</sup>

(115) Amin, S.; Balanikas, G.; Huie, K.; Hussain, N.; Geddie, J. E.; Hecht, S. S. *J. Org. Chem.* **1985**, *50*, 4642–4646.

(116) Turro, N. J. *Modern Molecular Photochemistry 1991*; University Science: Mill Valley, CA, 1991; Chapter 4.

Therefore, it was likely that the absorption bands of **12** at 436, 411, and 390 nm were corresponding to 0–0, 0–1, and 0–2 transitions, respectively. Similarly, the absorption bands of **8–11** at about 450, 426, and 407 nm were corresponding to 0–0, 0–1, and 0–2 transitions, respectively. However, in comparison with **12**, both major absorption bands of **8–11** red-shifted about 20 nm owing to the increase of effective conjugation length with the introduction of aromatic substituents. The absorption spectra of **8** and **10** exhibited a slight red-shift compared to those of **9** and **11**. This was compatible with the effect of methoxy substitution in the phenyl unit. The *o*-methoxy and *p*-methoxy groups diminish the energy difference between LUMO and HOMO more effectively and thus cause the red shift of adsorption and emission spectra. However, the *m*-methoxy group did not cause any difference in absorption and emission spectra of **9** compared to those of **11** that has no methoxy substituents, indicating little extension in effective conjugated length.

As shown in Figure 2, the emission  $\lambda_{\max}$  of **8–11** red-shifted about 20 nm in comparison with that of **12**. For **12**, the emission  $\lambda_{\max}$  peaked at 448 nm ( $22\,321\text{ cm}^{-1}$ ) with a vibronic peak at 470 nm. The wavenumber separation ( $615\text{ cm}^{-1}$ ) between absorption at 436 nm and emission  $\lambda_{\max}$  at 448 nm was less than that of vibronic absorption bands ( $1394\text{ cm}^{-1}$ ). According to the theoretical model of an anharmonic oscillator,<sup>116</sup> it might indicate that the emission band of **12** at 448 nm was corresponding to a 0–0 transition. Similarly, the emission bands of **8–11** at ca. 470 nm were corresponding to 0–0 transitions. The emission  $\lambda_{\max}$  of **8** and **10** all red-shifted several nanometers relative to those of **9** and **11**, similar to what has been observed in their absorption spectra. The emission features of **8** were the same as those of **10**, while the emission features of **9** were same as those of **11**. In comparison with **4–7**, the emission  $\lambda_{\max}$  of **8–11** blue-shifted about 35–40 nm due to the formation of the more rigid skeleton after the cyclization.<sup>117</sup>

We also investigated their emission spectra at various concentrations and in thin films. As shown in Figure 3a, with an increase of the concentration of **8** in chloroform, after normalization, we found that the relative emission intensity of the shoulder at longer wavelength was continuously enhanced and finally dominated the emission behaviors, which might be due to the formation of the aggregates or excimers at high concentration. The exciton might be delocalized in the whole assembly through  $\pi$ – $\pi$  interaction and thus had a lower energy state than one localized in a single molecule.<sup>118</sup> The aggregation was also evidenced by the excitation spectra, consistent with a monomer–aggregate transformation when the concentration increased from  $1.0 \times 10^{-5}\text{ M}$  to  $1.0 \times 10^{-4}\text{ M}$ . Similar results were observed from the emission behaviors of **9–11**.

Figure 3 also shows the emission spectra of precipitates **8–11** evaporated from chloroform solutions (1 mg/mL). The emission  $\lambda_{\max}$  red-shifted relative to those of solutions of their corresponding compounds. This was natural because the molecules in solid states had tighter and closer intermolecular interaction, which would lower the energy of the exciton. For **8–11**, the emission  $\lambda_{\max}$  in drop-cast films red-shifted in comparison with those in the dilute solution, which was in accordance with larger aggregates in the solid state. Table 1 summarizes their photophysical properties both in solutions and in solids.

**TABLE 1.** Photophysical Properties of **2** and **4–11** in Dilute Solutions and in Solid States in Comparison with **12** and Fluoranthene

comps	$\lambda_{\text{abs}}/\text{nm}$ (log $\epsilon$ ) (CHCl <sub>3</sub> )	$\lambda_{\text{abs}}/\text{nm}$ (solid)	$\lambda_{\text{PL}}/\text{nm}$ (CHCl <sub>3</sub> )	$\lambda_{\text{PL}}/\text{nm}$ (evaporation)	$\lambda_{\text{PL}}/\text{nm}$ (drop-cast) <sup>a</sup>	$\Phi_{\text{F}}^b$
<b>2</b>	274 (4.45), 287 (4.40), 366 (4.11), 383 (4.11)	275, 330, 369, 386	467	/	486	/
<b>4</b>	298 (4.57), 313 (4.40), 369 (4.15), 384 (4.15)	300, 313, 372, 388	513	/	492	/
<b>5</b>	299 (4.73), 367 (4.23), 384 (4.20)	301, 370, 387	499	/	485	/
<b>6</b>	300 (4.76), 369 (4.26), 384 (4.23)	303, 372, 388	510	/	503	/
<b>7</b>	299 (4.77), 368 (4.25), 384 (4.23)	301, 371, 388	500	/	497	/
<b>8</b>	343 (4.95), 360 (4.96), 429 (4.52), 455 (4.58)	382, 453, 484	472	526	524	0.16
<b>9</b>	341 (4.85), 357 (4.88), 426 (4.41), 452 (4.48)	380, 444, 475	465	531	513	0.23
<b>10</b>	343 (4.75), 361 (4.79), 427 (4.32), 454 (4.36)	376, 448, 478	470	518	518	0.18
<b>11</b>	340 (4.88), 355 (4.92), 424 (4.41), 450 (4.51)	370, 442, 472	465	508	510	0.23
<b>12</b>	289 (3.62), 302 (3.63), 341 (3.86), 390 (3.07), 411 (3.27), 436 (3.38)	/	448	/	/	/
fluoranthene	289 (4.69), 324 (3.92), 344 (4.03), 360 (4.04)	/	443, 463	/	/	/

<sup>a</sup> From chloroform solution ( $10^{-4}\text{ M}$ ). <sup>b</sup>  $\Phi_{\text{F}}$  of compounds **8–11** were measured in chloroform using 9,10-diphenylanthracene (in cyclohexane,  $\Phi_{\text{F}} = 1.00$ ) as reference.

**Thermal Properties.** Thermal properties of semiconductors **8–11**, which were crucial for thermal annealing and device performance, were measured by differential scanning calorimetry (DSC), and the curves from the heating (negative heat flow, downward peaks)/cooling (positive heat flow, upward peaks) cycle are shown in Figure 4 (corresponding data are compiled in Table 2). Melting points were estimated from the onset of the endothermic peaks (negative heat flow), and fusion enthalpies were calculated from the integration of the melting curves. All these four compounds exhibit good thermal stability with melting temperatures above  $250\text{ }^{\circ}\text{C}$  (decomposition temperatures are approximately  $400\text{ }^{\circ}\text{C}$  under a nitrogen atmosphere measured by thermal gravimetric analysis). Melting/crystallization processes were reversible through several heating/cooling cycles, while neither a glass state nor a liquid crystal (LC) phase transition was observed from the tests. These results are attributed to the short length of the flexible alkyl chains in

(117) Peaden, P. A.; Lee, M. L.; Hirata, Y.; Novotny, M. *Anal. Chem.* **1980**, *52*, 2268–2271.

(118) Schwab, A. D.; Smith, D. E.; Rich, C. S.; Young, E. R.; Smith, W. F.; de Paula, J. C. *J. Phys. Chem. B* **2003**, *107*, 11339–11345.

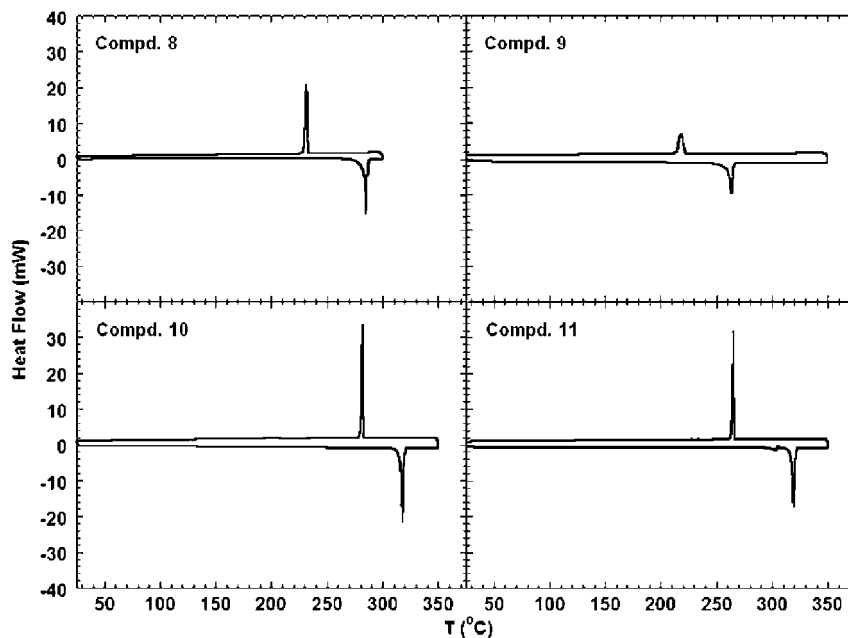


**FIGURE 4.** Differential scanning calorimetry curves of powder of compounds **8–11**. Upward peaks indicate endothermic processes, while downward peaks indicate exothermic processes. Scan rate: 10 deg/min.

**TABLE 2.** Thermal and Electrochemical Properties

comps	endothermic peak onset (°C)	$\Delta H_{fus}$ (kJ·mol <sup>-1</sup> )	$E_{ox}$ (V)	HOMO (eV)	mp (°C)
<b>8</b>	283	52	0.81	-5.69	285.5–286.5
<b>9</b>	260	44	0.93	-5.81	268–269
<b>10</b>	315	51	0.82	-5.70	>320
<b>11</b>	316	45	0.99	-5.87	>320

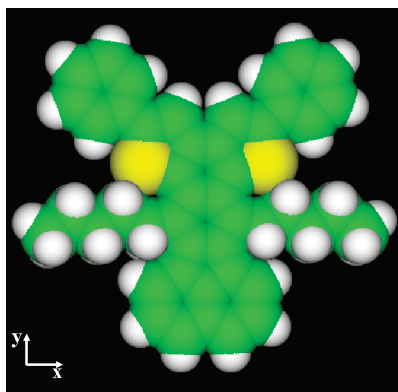


**FIGURE 5.** Molecular model of compound **11** optimized by the MM3 + UFF method. Molecular dimensions:  $x$ , 1.69 nm;  $y$ , 1.54 nm.

compounds **8–11**. According to the molecular model (Figure 5), the alkyl chains are on longer than rigid aromatic skeletons. Therefore, the alkyl side chain might not provide enough flexibility to form a liquid crystal phase.<sup>119</sup> As neither a glass state nor a LC phase transition was observed for semiconductors **8–11**, thermal annealing experiments were conducted below the melting temperatures.

**Electrochemical Properties in the Solid State.** In the case of organic  $p$ -type semiconducting materials where charge transport occurs predominantly by hopping through HOMOs, the relative HOMO energetic positions are crucial in determination of the injection of holes from the electrodes to the active

layer, consequently affecting the threshold voltage of the OFET devices.<sup>120</sup> The HOMO energies for semiconductors **8–11** in the solid state were estimated by conventional electrochemical techniques: cyclic voltammetry (CV) of drop casting films of compounds **8–11** performed in CH<sub>3</sub>CN (Figure 6), in which  $n$ -Bu<sub>4</sub>NPF<sub>6</sub> was used as the supporting electrolyte. All compounds showed partially reversible oxidation waves yielding radical cations, and HOMO levels of thin films were determined using the onset positions of the oxidation peaks, which were internally referenced to ferrocene's HOMO level (Table 2). Methoxy substituents at the outer benzene rings resulted in an increase in the HOMO levels, as we observed in **8–10** compared to **11**. Methoxy groups at *ortho*- and *para*-positions of the benzene rings can conjugate more effectively with the aromatic cores than that at *meta*-positions, causing the HOMO levels of **8** and **10** to be higher than that of **9**. These results are consistent with UV–vis absorption spectra.

**Thin Film Fabrication and Characteristics. Vacuum Deposition and Thermal Annealing of the Thin Films.** Semiconductors **8–11** were vacuum-evaporated onto  $n$ -octadecyltrichlorosilane (OTS) treated Si/SiO<sub>2</sub> substrate at  $4 \times 10^{-4}$  Pa at a rate of 0.1 nm s<sup>-1</sup> to form thin films (ca. 50 nm thick) as active layers in transistors. The enhancement of OFET device performance could be realized via the two most common methods: raising the temperature of substrate during small-molecule active layer materials vacuum deposition and thermal annealing after active layer materials solution deposition. Thermal annealing was often employed after semiconductor film was formed by spin casting a solution of polymer or small-molecule materials onto substrates.<sup>36,55,62,74,121–124</sup> This process requires materials to have a glass state or liquid crystal phase upon heating in general. Small molecules such as pentacene that do not have flexible alkyl chains do not undergo such a phase transition process. Compounds like pentacene and perylene diimides are often vacuum-deposited onto heated substrates,

(119) Etchegoin, P. *Phys. Rev. E* **1997**, *56*, 538–548.

(120) Zaumseil, J.; Sirringhaus, H. *Chem. Rev.* **2007**, *107*, 1296–1323.

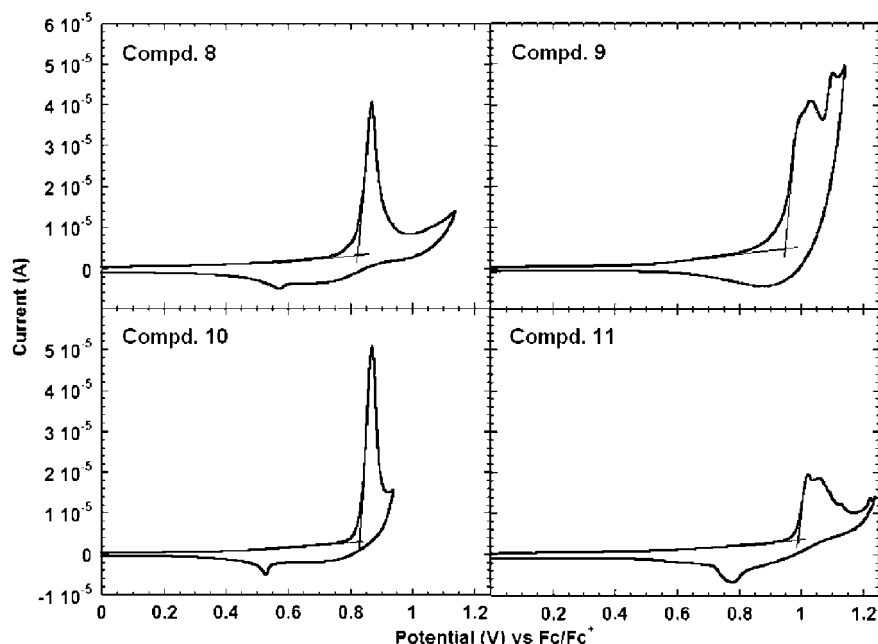


**FIGURE 6.** Cyclic voltammograms of drop casting films of compounds 8–11. Scan rate, 100 or 150  $\text{mV s}^{-1}$ ; working electrode, Pt disk; auxiliary electrode, Pt wire; reference electrode, Ag/AgCl; supporting electrolyte  $\text{NBu}_4\text{PF}_6$  (0.1 M,  $\text{CH}_3\text{CN}$ ).  $\text{Fc}/\text{Fc}^+$  was used as the internal reference (0.36 V vs SCE). HOMO was estimated vs vacuum level:  $E_{\text{HOMO}} = -4.88 - E_{\text{ox}}^{106}$

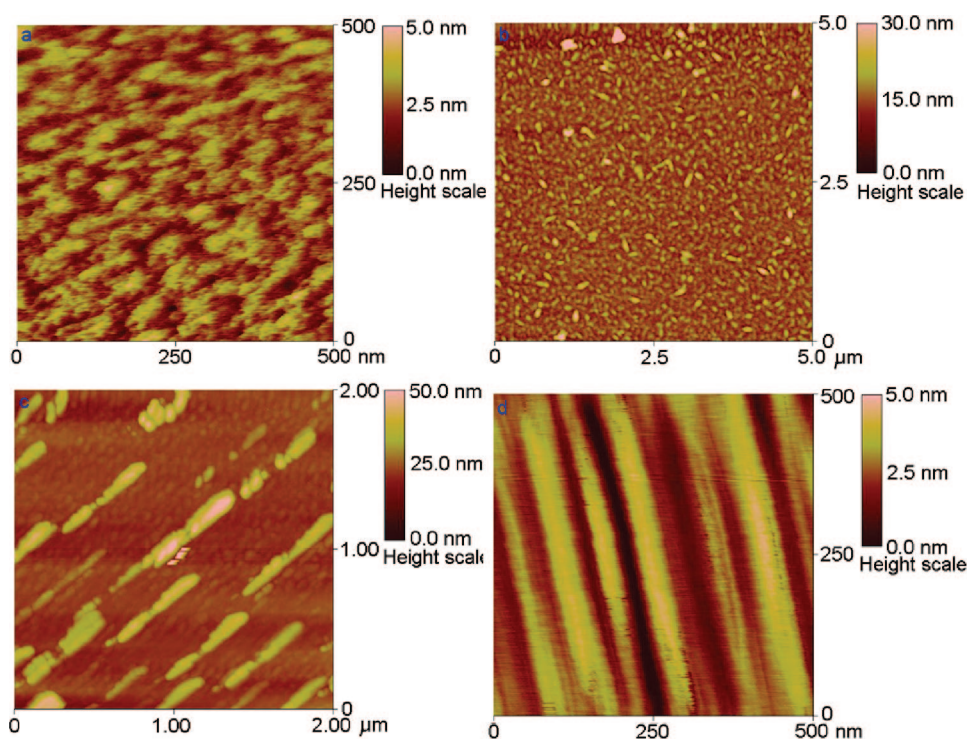


**FIGURE 7.** AFM images of pristine thin films of compounds 8–11: (a) 8, (b) 9, (c) 10, (d) 11.

without further treatment.<sup>12,106</sup> In our system, we used cold substrate (25 °C) to receive crystalline molecules in the gas phase to form thin films during vacuum deposition and then employed thermal annealing to align molecules on the OTS-treated  $\text{SiO}_2$  surface. When molecules in the gas phase came in contact with cold substrates, the molecules formed an amorphous

film consisting of microcrystalline grains (this was verified by X-ray diffraction experiments and atomic force microscope (AFM) images, which will be discussed in the next sections).

(123) Ong, B. S.; Wu, Y.; Liu, P.; Gardner, S. *Adv. Mater.* **2005**, *17*, 1141–1144.

(124) McCulloch, I.; Heeney, M.; Bailey, C.; Genevicius, K.; MacDonald, I.; Shkunov, M.; Sparrowe, D.; Tierney, S.; Wagner, R.; Zhang, W.; Chabinyc, M. L.; Kline, R. J.; McGehee, M. D.; Toney, M. F. *Nat. Mater.* **2006**, *5*, 328–333.

(125) Roduner, E. *Chem. Soc. Rev.* **2006**, *35*, 583–592.

(121) Salleo, A.; Arias, A. C. *Adv. Mater.* **2007**, *19*, 3540–3543.

(122) Chang, P. C.; Lee, J.; Huang, D.; Subramanian, V.; Murphy, A. R.; Fréchet, J. M. J. *Chem. Mater.* **2004**, *16*, 4783–4789.

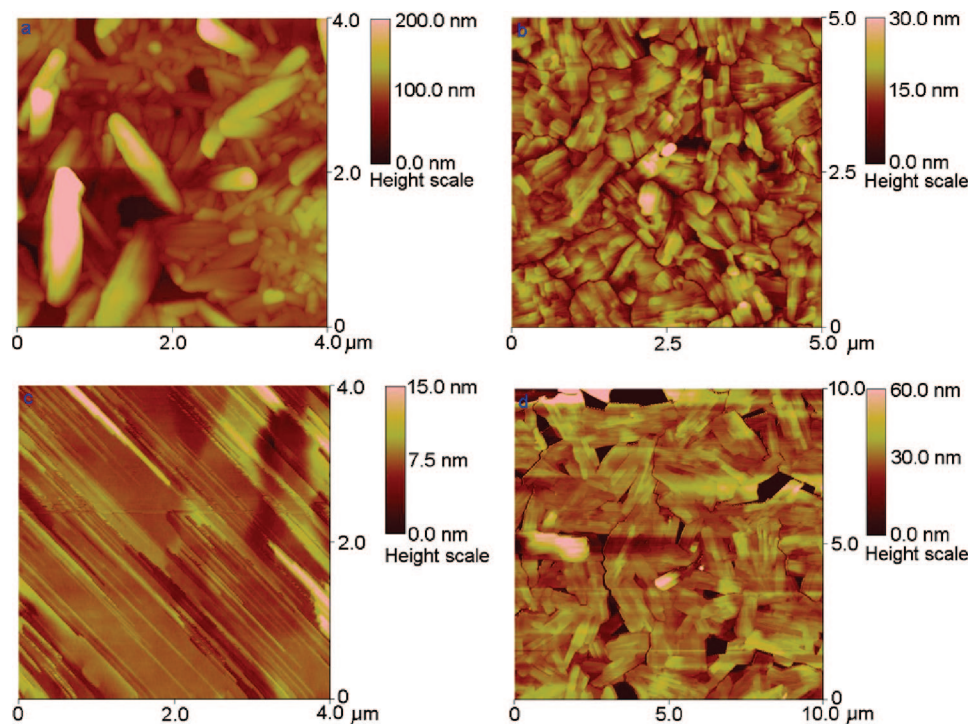


FIGURE 8. AFM images of thin films of compounds 8–11 after thermal annealing: (a) 8, (b) 9, (c) 10, (d) 11.

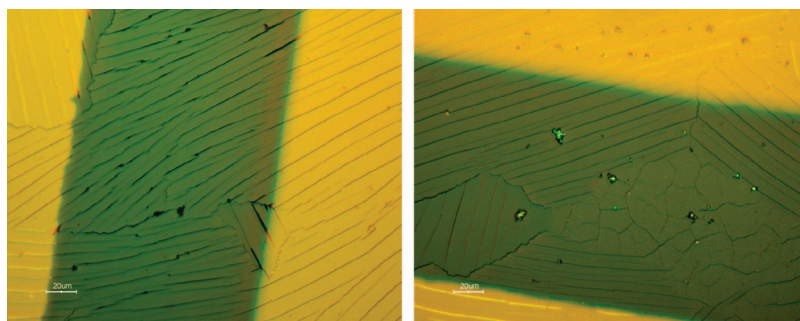


FIGURE 9. Optical microscopy images of thermal annealed films of 10. Scale bar: 20  $\mu\text{m}$ . Yellow region: gold metal. Green region: semiconducting materials.

Ultrathin films or crystals at nano size (50 nm) have lower melting temperature than the bulk materials caused by surface effect.<sup>125</sup> If the crystal melts upon heating, small crystals will combine together to form large crystals that have the small surface area driven by surface free energy, which will often cause “dewetting”.<sup>30</sup> Taking these into consideration, prior to gold metal electrode deposition, we conducted thermal annealing of these semiconductor films at approximately 40 °C below their bulk melting points under a nitrogen atmosphere for 20 min, followed by slowly cooling the thin films to 25 °C. Such a process is easier to carry out and more economic compared to elevating the temperature of substrates during vacuum deposition. In other words, this method demands simpler instruments because the vacuum system is less complicated if the substrate does not need heating. Also, a smaller amount of semiconductor sample is required because after a one-time vacuum deposition different temperatures can be applied during the thermal annealing process to achieve different device performance. Thermal annealing of these crystalline films effectively converted microcrystallines to larger connected crystalline grains with  $\pi$ -conjugated cores aligned approximately perpendicular to the dielectric surface (this was verified by X-ray diffraction

experiments and AFM images discussed below), which will favor hole transport in OFET devices.<sup>126–128</sup>

**Thin Film Morphology by AFM.** Topographical images of the films of semiconductors 8–11 newly vacuum-deposited and after thermal annealing obtained from AFM experiments were carefully investigated. Figures 7 and 8 shows AFM images of the vacuum-deposited films of 8–11 on OTS-treated  $\text{SiO}_2/\text{Si}$  substrates. Thermal annealing at proper temperatures effectively combined small crystalline grains into continuously connected large crystals. All films showed one transformation in common after thermal energy was provided under certain temperatures: increased grain size and decreased boundaries. This transformation would lead to hole-mobility enhancement, because higher defect concentration in grain boundaries of multicrystal thin films usually leads to poor carrier transport.<sup>127,128</sup>

The images of pristine films of 8 and 9 in Figures 7a and 7b indicated that these rough films consist of discontinuous islands

(126) Sun, Y.; Liu, Y.; Zhu, D. *J. Mater. Chem.* **2005**, *15*, 53–65.

(127) Bao, Z.; Lovinger, A. J.; Dodabalapur, A. *Adv. Mater.* **1997**, *9*, 42–44.

(128) Bao, Z.; Lovinger, A. J.; Brown, J. *J. Am. Chem. Soc.* **1998**, *120*, 207–208.

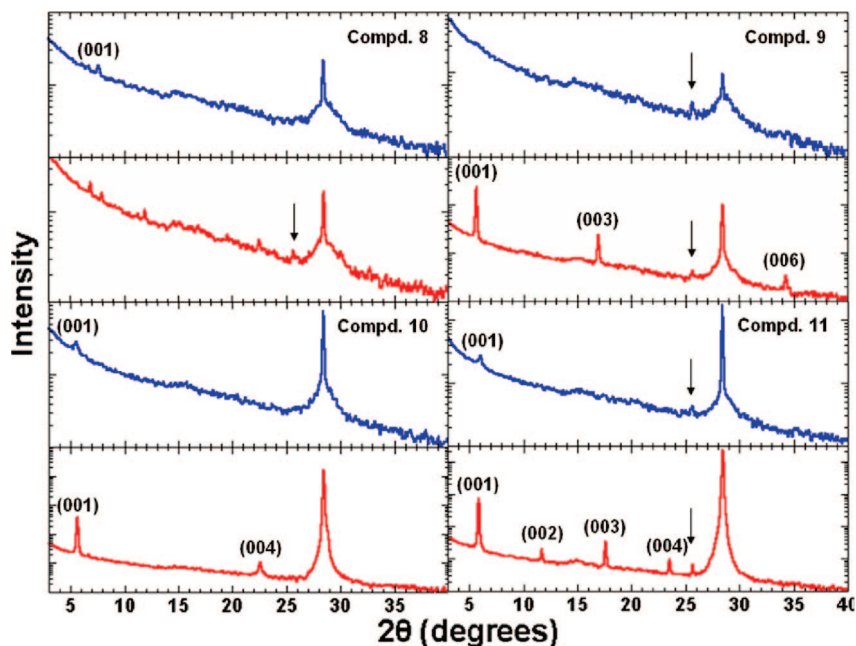


**FIGURE 10.** X-ray diffraction pattern of vacuum-deposited films of compounds **8–11**: blue lines in the upper halves, before thermal annealing; red lines in the bottom halves, after thermal annealing. The diffraction peak at  $2\theta = 28.44^\circ$  with huge intensity is due to the  $\text{SiO}_2/\text{Si}$  substrate.

**TABLE 3.** *d*-Spacing Calculated from  $2\theta$  Diffraction Peaks of Films of **8–11** and Performance Parameters of OFETs Based on These Films

comps	pristine film				annealed film			
	<i>D</i> (nm)	$\mu$ ( $\text{cm}^2 \text{V}^{-1} \text{s}^{-1}$ )	$V_{\text{th}}$ (V)	$I_{\text{on}}/I_{\text{off}}$	<i>D</i> (nm)	$\mu$ ( $\text{cm}^2 \text{V}^{-1} \text{s}^{-1}$ )	$V_{\text{th}}$ (V)	$I_{\text{on}}/I_{\text{off}}$
<b>8</b>	1.16	$2 \times 10^{-5}$	−1.4	$6 \times 10^2$	N.D. <sup>a</sup>	$2.6 \times 10^{-3}$	−5.9	$5 \times 10^5$
<b>9</b>	N.D. <sup>a</sup>	$7 \times 10^{-5}$	−9.8	$1 \times 10^4$	1.57	$4.9 \times 10^{-3}$	−12.6	$7 \times 10^5$
<b>10</b>	1.60	$1.7 \times 10^{-4}$	−33	$2 \times 10^2$	1.57	$3.5 \times 10^{-3}$	8.5	$2 \times 10^3$
<b>11</b>	1.46	$7.7 \times 10^{-3}$	−11	$1 \times 10^5$	1.50	0.083	−37	$3 \times 10^6$

<sup>a</sup> Not determined.

with the size of ca.  $0.1 \mu\text{m}$ . After annealing for 20 min, isolated grains combined into larger crystalline grains connected to each other with the size of ca.  $0.5 \mu\text{m}$ . The longest crystal had the length of ca.  $1 \mu\text{m}$  and an aspect ratio of approximately 10, as shown in Figures 8a and 8b, resulting in increased grain size and decreased grain boundaries. The AFM images in Figures 7c and 7d of the pristine films of **10** and **11** obviously showed one-dimensional nanostructures, which can be attributed to stronger one-dimensional elongation trends of these two molecules' crystals compared to **8** and **9**. These one-dimensional elongation trends, resulting from  $\pi$ – $\pi$  stacking between aromatic cores, would lead to improved charge carrier mobility in transistor devices, proved by theoretical calculations and experimental results,<sup>25,47,129</sup> (supported by the OFET characterization of films before thermal annealing). After thermal annealing at  $270^\circ\text{C}$  for 20 min, the film of **11** was composed of the largest crystalline grains among these four compounds with the size of ca.  $2.0$  (maximum size  $5 \mu\text{m}$ ) close to each other, which indicated that crystalline boundaries were effectively decreased and would enhance OFET performance consequently.

The most interesting images were obtained from the films of **10**, shown in Figure 7c and 8c. Thermal annealed films of **10**,

which would be used as the TFT (thin film transistor) active layer, exhibited a highly ordered one-dimensional nanostructure with length approaching the magnitude of micrometer indicated by the scale bar. Notably, it is very rare that this kind of ordered one-dimensional nanostructure can be achieved through simple vacuum deposition of the materials onto bare OTS-treated  $\text{SiO}_2/\text{Si}$  substrate, without introducing materials such as *para*-hexaphenyl<sup>88</sup> or an advanced film fabrication technique such as zone casting.<sup>23</sup> As optical microscope pictures taken from a larger area of the same region for AFM are shown in Figure 9, the ordered nanostructure of **10** associates into macroscale channels with a length of ca.  $100 \mu\text{m}$ . However, unfortunately, the nanostructures were grown heading random directions within the substrate plane. As shown by the picture on the right side, we concluded both of the one-dimensional structures in the direction nearly parallel to the gold electrode edge along with one-dimensional channels that intersected would countercheck charge transporting in OFET and lead to a hole mobility lower than expected.

**Thin Film X-ray Diffraction.** X-ray diffraction experiments have been carried out to acquire insight into the microstructure of the vacuum deposited thin films of the semiconductors **8–11**. We carefully compared the diffraction patterns of the films before and after thermal annealing to understand the change of the microstructures, which would affect charge transport properties of organic thin films in transistor devices. X-ray diffraction scans are utilized to obtain out-of-plane *d*-spacings in the films,

(129) Miao, Q.; Lefenfeld, M.; Nguyen, T. Q.; Siegrist, T.; Kloc, C.; Nuckolls, C. *Adv. Mater.* **2005**, *17*, 407–412.

(130) Pal, M.; Kundu, N. G. *J. Chem. Soc., Perkin Trans. 1* **1996**, *5*, 449–452.

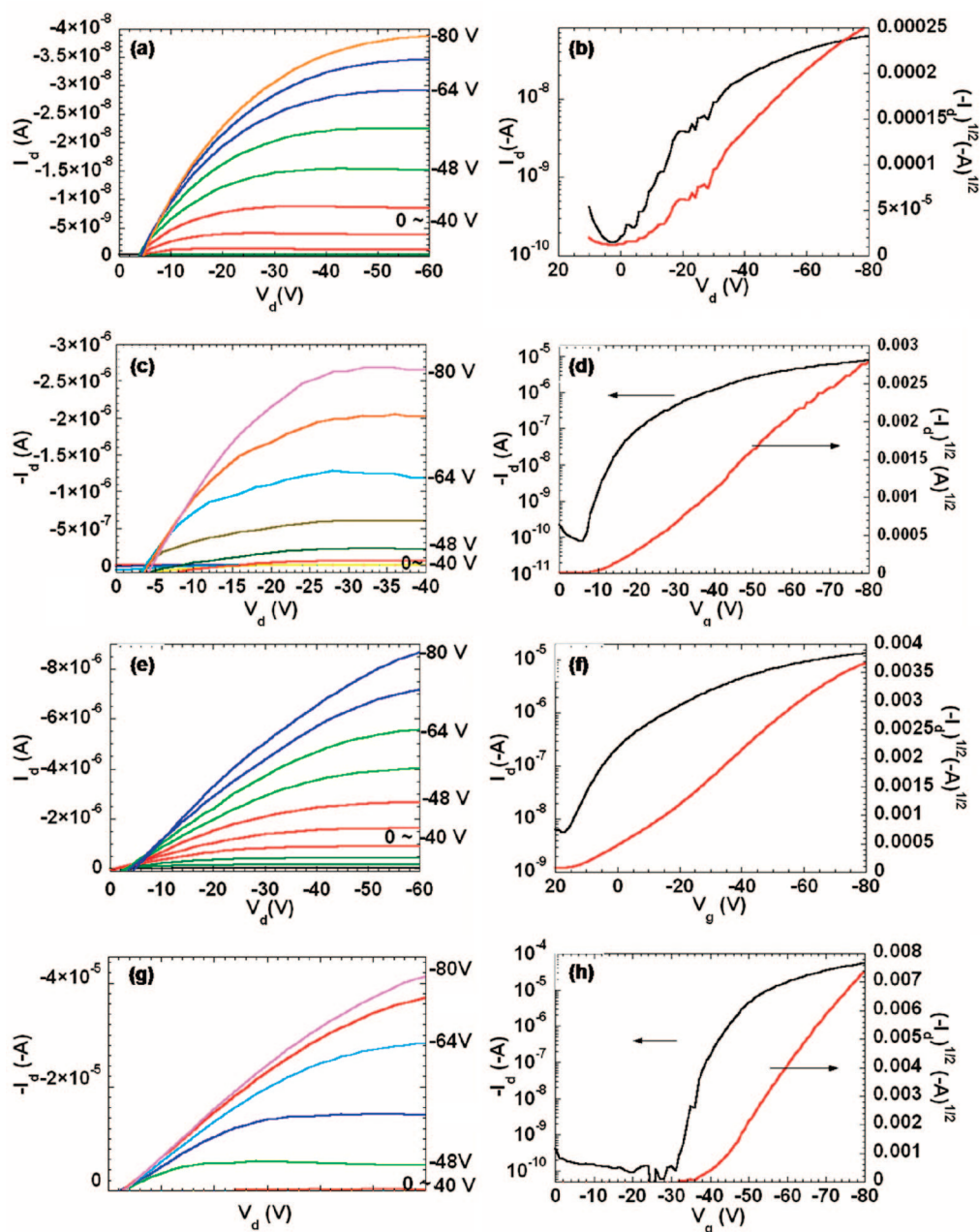


**FIGURE 11.** Electrical characterization of OFETs based on **8–11** after thermal annealing. (a), (c), (e), (g): output curves of **8–11** taken at different gate voltages, respectively. (b), (d), (f), (h): transfer curves of **8–11** at constant  $V_D = -60$  V, respectively.

which allow us to determine the molecular orientations relative to the substrate surface. As shown in the upper halves in Figure 10, it was quite difficult to find any sharp diffraction peaks in the pristine films, which indicated the crystalline quality of these polycrystalline organic thin films was very poor. Only first-order diffraction peaks around  $2\theta = 5^\circ$  with very low intensity were observed in pristine films of **8**, **10**, and **11**. But  $d$ -spacings of 0.347 nm calculated from diffraction small peaks at  $2\theta = 25.7^\circ$  (arrow pointed), which were typical distances of  $\pi$ - $\pi$  interactions, showed up in the XRD patterns of pristine films of **9** and **11**. The observation of these diffraction peaks could be due to the molecules lying on the substrates in different orientations in pristine films. After thermal annealing, the quality of crystalline of these films improved remarkably, which was confirmed by the increased intensity of diffraction peaks. Except **8**, annealed films of **9–11** exhibit several peaks for the

predominating phases, which have  $d$ -spacings of nearly 1.6 nm (calculated  $d$ -spacings are summarized in Table 3). These  $d$ -spacings, which were assignable to  $(00h)$  reflections,<sup>45</sup> were close to the molecular dimensions obtained from the molecular model, and we could judge that the aromatic cores of the molecules are aligned approximately perpendicular to the SiO<sub>2</sub>/Si surface in the predominating phase.<sup>4</sup> Molecule **8**, due to its torsional strain introduced by the *ortho*-methoxy group, might not stack so effectively as other isomers, resulting in a less-ordered crystalline structure.

**Field-Effect Transistor Characterization.** Organic field-effect transistor devices using **8–11** as the active layers were fabricated in a top-contact configuration to analyze the materials' charge transport characteristics via evaluation of the current–voltage response. Three performance parameters were extracted from the FET  $I$ – $V$  response curves: the charge carrier mobility ( $\mu$ ),

current on–off ratio ( $I_{\text{on}}/I_{\text{off}}$ ), and threshold voltage ( $V_{\text{th}}$ ). Both newly deposited films and thermal annealed films of **8–11** were employed as active layers in FET devices after gold metal was vacuum-deposited as an electrode. All OFET devices were tested under ambient condition several times, and their performance remained persistent over two weeks (stored in air), indicating the high stability of these transistors based on **8–11**. In this contribution, we proved that thermal annealing is an efficient method to improve the transistor device performance based on crystalline small molecules without the glass state or LC phase: both hole mobility and on/off current ratio in annealed films were several orders of magnitude larger than that in newly deposited films. (Performance data are summarized in Table 3, and output and transfer curves of annealing films of **8–11** are depicted in Figure 11.) These device performance improvements are expected as results of increased grain size and higher crystalline quality of active layers, which were verified by AFM and XRD, respectively. The threshold voltages of the transistor device based on annealed films of **8–11** are  $-5.9$ ,  $-12.6$ ,  $8.5$ , and  $-37$  V, respectively.  $V_{\text{th}}$  values of semiconductor films of **8–11** are in good agreement with CV results: the higher the HOMO levels are, the easier the molecules are oxidized and the easier the holes are injected from electrodes. The trends of mobility of semiconductor films of **8–11** are in the sequence **11** > **9**, **10** > **8**, which is consistent with AFM and XRD results: the higher the quality of crystalline is, the easier holes are transported. Some conclusions regarding structure–property relationships could be drawn from the transistor performance parameters and data gathered from AFM and XRD experiments. First, methoxy groups at *ortho*-positions, which would lead to a larger torsion angle between the outer benzene ring and rigid core compared to that at *meta*- and *para*-positions, caused less-ordered crystalline structure on the substrate, disfavoring charge carrier transporting. Second, decreased quality of crystalline caused by methoxy substitution would lower the mobilities of transistors. As a result of these two reasons, the best performance was realized from **11**. Hole mobility in annealed films of **11** could reach as high as  $0.083 \text{ cm}^2 \text{ V}^{-1} \text{ s}^{-1}$ , along with the current on/off ratio of  $10^6$ , without further device optimization. These results indicate that our novel fluoranthene-based compounds are promising candidates for organic field-effect transistor active layer materials.

## Conclusions

In summary, we have developed a facile approach to a new family of air-stable sulfur-hetero oligoarenes containing the benzo[*k*]fluoranthene unit through the reaction sequence of the Diels–Alder reaction, decarbonylation, and  $\text{FeCl}_3$ -oxidative cyclization. In comparison with their corresponding precursors **4–7** in dilute solutions, the absorption  $\lambda_{\text{max}}$  of **8–11** red-shifts after the formation of a larger polycyclic aromatic skeleton; however, their emission  $\lambda_{\text{max}}$  blue-shifts, which demonstrates

that such a conjugated skeleton is very rigid. OFETs based on thin films of **8–11** have been fabricated. As shown by Figures 8c and 9, long-range one-dimensional nanostructures achieved previously only by means of inducing layers or zone-casting can now be realized via chemical engineering. Substituents at different positions on the same conjugated aromatic core in **8–11** affect the HOMO levels, quality of crystalline, and film morphologies, consequently influencing transistor performance. More specifically, the structure–property relationships could be deduced from our experimental result. Decreasing crystalline degree caused by methoxy groups would lower the charge carrier mobility in FET devices. The thermal annealing process is an efficient way to decrease the grain boundary and increase the crystalline degree. The performance of thin film transistors has been remarkably improved by means of thermal annealing developed by our group, which provides a new possibility in fabricating OFET devices.

## Experimental

**Fabrications of Organic Films and OFETs.** Organic field-effect transistors based on fluoranthene derivatives **8–11** were fabricated in a “top contact” configuration. A heavily doped, *n*-type Si wafer was used as the gate electrode and substrate. A thermally grown  $\text{SiO}_2$  layer (ca. 300 nm thick) acted as a gate insulator with a unit capacitance of  $11 \text{ nF cm}^{-2}$ . Prior to the deposition of semiconductors, the Si/ $\text{SiO}_2$  substrate was immersed in 10 mg/mL *n*-octadecyltrichlorosilane (OTS) in toluene at  $60^\circ\text{C}$  for 20 min. Semiconductors **8–11** were vacuum-evaporated onto Si/ $\text{SiO}_2$  substrate at  $4 \times 10^{-4} \text{ Pa}$  at a rate of  $0.1 \text{ nm s}^{-1}$  to form thin films (ca. 50 nm thick) as active layers. Source and drain electrodes (ca. 100 nm thick) were prepared by deposition of Au with a shadow mask. The defined channel width ( $W$ ) and channel length ( $L$ ) were 100  $\mu\text{m}$  and 10 mm, respectively. The annealing procedure was done before the deposition of Au under nitrogen. Thin films of semiconductors **8–11** were thermally annealed at 240, 235, 230, and  $270^\circ\text{C}$  for 20 min, respectively.

**Characterization of Thin Film OFETs.** The thin films of semiconductors were imaged with the tapping mode of AFM. The organic transistors were tested under ambient condition at room temperature. Field-effect mobilities ( $\mu_{\text{FET}}$ ) were extracted from the saturation region of  $I_{\text{d}}$  using the equation  $I_{\text{d}} = (WC_i/2L)\mu_{\text{FET}}(V_{\text{g}} - V_{\text{th}})^2$ .

**Acknowledgment.** This research was financially supported by the Major State Basic Research Development Program (No. 2006CB921602 and 2007CB808000) from the Minister of Science and Technology and by the National Natural Science Foundation of China.

**Supporting Information Available:** Synthesis details and  $^1\text{H}$  and  $^{13}\text{C}$  NMR spectra of all new compounds **2–12** (PDF). This material is available free of charge via the Internet at <http://pubs.acs.org>.

JO800606B